Research article

Hanlyun Cho, Younghwan Yang, Dasol Lee, Sunae So and Junsuk Rho*

# Experimental demonstration of broadband negative refraction at visible frequencies by critical layer thickness analysis in a vertical hyperbolic metamaterial

https://doi.org/10.1515/nanoph-2021-0337
Received July 2, 2021; accepted September 7, 2021;
published online September 22, 2021

**Abstract:** This work presents a vertical hyperbolic metamaterial (vHMM) consisting of a vertically stacked metal-dielectric multilayer that operates in the visible spectrum. The vHMM is designed by exploiting the relation between negative refraction and effective permittivity along the perpendicular direction of the layers ($\varepsilon_\perp$). When a vHMM has a high loss tangent defined by $\tan\delta_\perp \equiv \mathrm{Im}(\varepsilon_\perp)/\mathrm{Re}(\varepsilon_\perp)$, even a vHMM composed of relatively thick layers can generate negative refraction. A fabricable vHMM composed of gold and copolymer resist (EL8) which exhibits negative refraction at the wavelengths between 450 and 550 nm is designed using critical layer thickness analysis. The largest negative refraction is observed at the wavelength of 500 nm, where the angle of refraction reaches −1.03°. The corresponding loss tangent and equivalent refractive index are 1.08 and −0.47, respectively. However, negative refraction is not observed at the wavelengths longer than 550 nm due to low $\tan\delta_\perp$. We uncover that the $\tan\delta_\perp$ of a vHMM is the dominant condition for generating negative refraction rather than the ratio of layer thickness to wavelength.

**Keywords:** critical layer thickness; effective permittivity; focused ion-beam; hyperbolic metamaterial; negative refraction.

## 1 Introduction

Hyperbolic metamaterials (HMMs) have extraordinary optical properties as a consequence of the hyperbolic shape of the isofrequency surface [1–4]. The hyperbolic dispersion of the HMM provides numerous unusual characteristics including negative refraction [5–15], sub-wavelength-resolution imaging [16–24], observation of the optical spin Hall effect [25, 26], anomalous scaling laws [27], thermal emission [28, 29], multidimensional images [30], extreme mechanical hardness [31], biochemical sensing [32–36], excitation of surface waves [37], excitation of high-k modes [38], and perfect absorption [39, 40].

The negative refraction using HMMs has been mainly studied by considering multilayered stacks of horizontal metal and dielectric layers, i.e., horizontal HMMs (hHMMs) [5–14]. If the thickness of each layer is sufficiently small compared to the wavelength of the incident light ($\lambda$), then the hyperbolic dispersion relation of the hHMM can be explained by effective medium theory (EMT) [41, 42]. However, the working frequency ranges for the negative refraction of the hHMMs are generally narrow as the hyperbolic dispersion is a consequence of optical resonances [43]. This limits the negative refraction to occur only near the resonance frequency.

Multilayered structures composed of vertical alternating metal and dielectric layers, i.e., vertical HMMs (vHMMs), have been proposed as a solution to overcome

***Corresponding author: Junsuk Rho**, Department of Mechanical Engineering, Pohang University of Science and Technology (POSTECH), Pohang, 37673, Republic of Korea; Department of Chemical Engineering, Pohang University of Science and Technology (POSTECH), Pohang, 37673, Republic of Korea; POSCO-POSTECH-RIST Convergence Research Center for Flat Optics and Metaphotonics, Pohang, 37673, Republic of Korea; and National Institute of Nanomaterials Technology (NINT), Pohang, 37673, Republic of Korea, E-mail: jsrho@postech.ac.kr. https://orcid.org/0000-0002-2179-2890

**Hanlyun Cho, Younghwan Yang and Sunae So,** Department of Mechanical Engineering, Pohang University of Science and Technology (POSTECH), Pohang, 37673, Republic of Korea, E-mail: hanlyun.cho@postech.ac.kr (H. Cho), younghwan@postech.ac.kr (Y. Yang), ssa1021@postech.ac.kr (S. So). https://orcid.org/0000-0001-6479-6966 (H. Cho). https://orcid.org/0000-0003-2173-4217 (Y. Yang). https://orcid.org/0000-0001-8606-2234 (S. So)

**Dasol Lee,** Department of Mechanical Engineering, Pohang University of Science and Technology (POSTECH), Pohang, 37673, Republic of Korea; and Department of Biomedical Engineering, Yonsei University, Wonju, 26493, Republic of Korea, E-mail: dasol@yonsei.ac.kr

the limitation of the hHMMs [25, 43]. However, the fabrication of vHMMs that exhibit negative refraction at visible frequencies is extremely difficult as the structures' layers must be sufficiently thin to demonstrate the hyperbolic dispersion. Nano trench structures with a high aspect ratios (AR) up to 20 have been reported but operate in the mid-infrared range [32, 37] or only the reflectance of the structure has been reported [44]. To overcome this difficulty, vHMMs composed of metal and air have been proposed [25, 45], but the negative refraction has not been studied. Recently, a critical layer thickness of the vHMM has been proposed to be the maximum layer thickness divided by $\lambda$ at which the negative refraction occurs [46]. The critical layer thickness is related to the effective permittivity along the perpendicular direction of the layer ($\varepsilon_\perp$) of the vHMM. The critical layer thickness tends to increase as the value of $\mathrm{Im}(\varepsilon_\perp)/\mathrm{Re}(\varepsilon_\perp)$ increases. Therefore, vHMMs with relatively thick layers can exhibit hyperbolic dispersion and provide negative refraction, if the loss tangent defined by $\tan\delta_\perp \equiv \mathrm{Im}(\varepsilon_\perp)/\mathrm{Re}(\varepsilon_\perp)$ is sufficiently high.

In this study, a vHMM composed of gold and copolymer resist (EL8) is experimentally demonstrated to show negative refraction in visible frequencies. We use critical layer thickness analysis to find fabricable thicknesses of 150 nm and 100 nm for the gold and the dielectric layers, respectively. Despite the relatively large thickness of layers compared to $\lambda$, the vHMM exhibits hyperbolic dispersion to induce negative refraction and can be easily realized using a commercially focused ion-beam (FIB) milling method.

# 2 Methods

## 2.1 Simulation

Commercially available Comsol Multiphysics was used. The predefined free triangular mesh and extremely fine size were applied. The relative error estimate for every calculation was $<10^{-11}$.

## 2.2 Experiment

A supercontinuum laser (YSL, SC-Pro 7) was used for a light source. The beam was linearly polarized after a polarizer (LPVISE100-A) and reached the vHMM prism device. The light that transmitted through the vHMM was captured by a CCD camera (Lumenera, Infinity 2-1R). The angle of refraction was measured and obtained from the position of the captured image compared to the one without the vHMM.

# 3 Fundamentals of HMM

A vertically stacked metal-dielectric multilayered structure is a typical example of a vHMM (Figure 1(a)). If the vHMM has sufficiently thin layers, its permittivity can be calculated using EMT [47] as

$$\epsilon_\parallel = f\epsilon_d + (1-f)\epsilon_m\,, \tag{1}$$

$$\epsilon_\perp = \frac{\epsilon_d\epsilon_m}{f\epsilon_m + (1-f)\epsilon_d}\,, \tag{2}$$

$$f = \frac{d_d}{d_d + d_m}, \tag{3}$$

where $\varepsilon_\parallel$ is the effective permittivity along the parallel direction of the layers; $\varepsilon_d$ and $\varepsilon_m$ are permittivities of the dielectric and metallic materials, respectively; $f$ is the filling ratio of the dielectric to the vHMM; and $d_d$ and $d_m$ are the dielectric and metallic layer thicknesses, respectively.

When transverse-magnetic polarized light is incident, the dispersion relation of the HMM is described as [3]

$$\frac{k_x^2}{\epsilon_\parallel} + \frac{k_y^2 + k_z^2}{\epsilon_\perp} = k_0^2 = \left(\frac{\omega}{c}\right)^2, \tag{4}$$

where $k_x$, $k_y$, and $k_z$ are the $x$, $y$, and $z$-directional wave vectors in the HMM, $k_O$ is the wave vector in a vacuum, $\omega$ is the angular frequency, and $c$ is the speed of light in a vacuum. The direction of $\varepsilon_\perp$ is parallel to the $x$-direction. Equation (4) shows a hyperbolic isofrequency surface if the signs of $\mathrm{Re}(\varepsilon_\parallel)$ and $\mathrm{Re}(\varepsilon_\perp)$ are different (Figure 1(b)). The

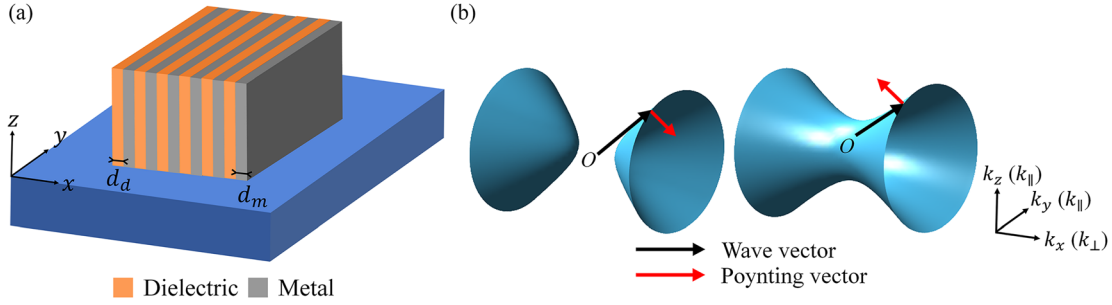


**Figure 1:** Characteristics of vHMM.
(a) Schematics of a vertically stacked hyperbolic metamaterial (vHMM). The $x$-direction is perpendicular to the layers. (b) Isofrequency surfaces of a type-I HMM (left) and a type-II HMM (right). The vHMM is a type-II HMM. The wave vector and the Poynting vector of the type-II HMM have different signs along the $x$-direction; this characteristic implies that the vHMM can provide negative refraction.

wave vector and Poynting vector therefore have opposite signs, which indicates negative refraction [13]. If $\mathrm{Re}(\varepsilon_{\parallel})$ is positive, the HMM is classified as type-I; with hHMMs being a typical example, while if $\mathrm{Re}(\varepsilon_{\parallel})$ is negative, the HMM is classified as type-II; with vHMMs being an example of a type-II HMM.

# 4 Results and discussion

## 4.1 Design and fabrication

The biggest challenge to the fabrication of vHMMs that exhibit negative refraction at visible frequencies is that they must have both extremely thin layers and a high AR. Some previous studies considered the vHMM structure numerically, but practical the realization of the proposed structures is extremely difficult. One proposed vHMM is composed of aluminum and silicon dioxide with a layer thickness of 30 nm and AR = 50 [43]. Another was composed of silver and magnesium fluoride with a layer thickness of 18 nm and AR = 111 [46]. However, these structures cannot be fabricated using commercial fabrication techniques.

The working frequency range of the vHMM composed of gold and EL8 for the negative refraction is broad, and the hHMM composed of the same materials cannot provide negative refraction at any $\lambda$ (Figure 2(a)). Theoretically, the vHMM can provide negative refraction in the whole visible frequencies. In addition, the vHMM has a sufficiently high $\tan\delta_{\perp}$ at $\lambda \approx 500$ nm and $f = 0.4$ (Figure 2(b)). Therefore, the vHMM composed of gold and EL8 is suitable to demonstrate negative refraction experimentally. The relative permittivity of gold varies with wavelength and both $\mathrm{Re}(\varepsilon_m)$ and $\mathrm{Im}(\varepsilon_m)$ tend to decrease as the wavelength increases, but the relative permittivity of EL8 does not (Figure 2(c)). In the vHMM that has $f = 0.4$, $\mathrm{Re}(\varepsilon_{\parallel})$ is negative and $\mathrm{Re}(\varepsilon_{\perp})$ is positive in the whole range $450 \le \lambda \le 650$ nm (Figure 2(d)).

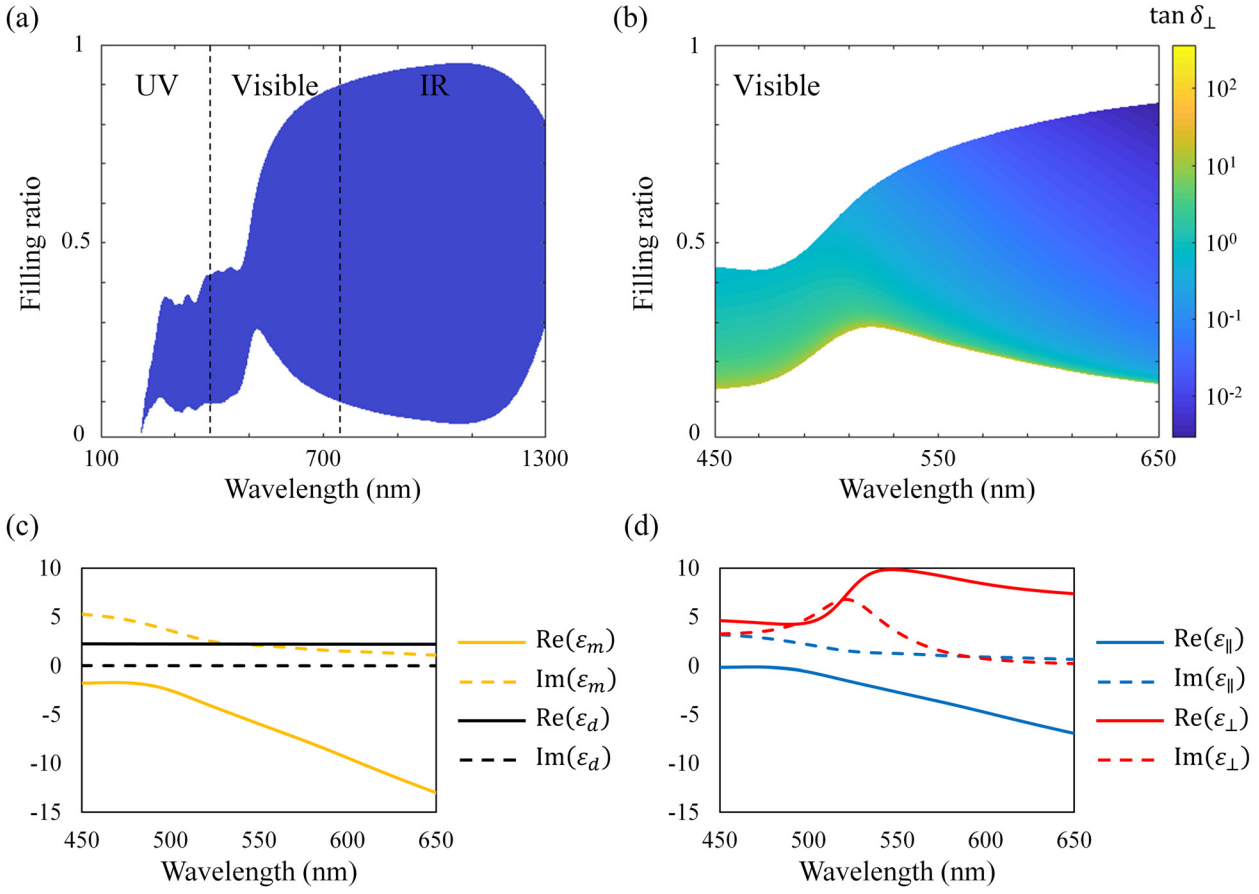


**Figure 2:** Properties of a vHMM composed of gold and EL8.
(a) Working frequency range of a vHMM composed of gold and EL8 for the negative refraction. The hHMM composed of the same materials cannot provide negative refraction. (b) $\tan\delta_{\perp}$ of the vHMM in the visible range. The vHMM that has a filling ratio $f = 0.4$ has a high $\tan\delta_{\perp}$ near $\lambda = 500$ nm. (c) Relative permittivities of gold (yellow lines) and EL8 (black lines). (d) Effective permittivity of the vHMM with the filling ratio $f = 0.4$.

$\mathrm{Im}(\varepsilon_\perp)$ increases in the range $450 \le \lambda \le 520$ nm, and $\mathrm{Im}(\varepsilon_\perp)$ is even larger than $\mathrm{Re}(\varepsilon_\perp)$ at $\lambda \approx 500$ nm. $\mathrm{Im}(\varepsilon_\perp)$ is sharply decreasing after $\lambda = 520$ nm where the slope of $\mathrm{Im}(\varepsilon_m)$ is gradual. If $\mathrm{Im}(\varepsilon_d)$ is negligible, $\tan\delta_\perp$ is expressed as

$$\tan\delta_\perp = \frac{(1-f)\mathrm{Im}(\epsilon_m)\mathrm{Re}(\epsilon_d)^2}{f\,\mathrm{Re}(\epsilon_m)^2\mathrm{Re}(\epsilon_d) + (1-f)\mathrm{Re}(\epsilon_m)\mathrm{Re}(\epsilon_d)^2 + f\,\mathrm{Im}(\epsilon_m)^2\mathrm{Re}(\epsilon_d)} \quad (5)$$

When the absolute value of $\mathrm{Re}(\varepsilon_\perp)$ is sufficiently larger than $\mathrm{Im}(\varepsilon_\perp)$, $\tan\delta_\perp$ becomes low. $\tan\delta_\perp$ can be measured by using total internal reflection ellipsometry [48].

The vHMM is fabricated using two-step FIB milling (FEI, Helios NanoLab 650) and polymer-resin spin-coating. Firstly, a 400 nm-thick layer of gold is deposited using an electron-beam evaporator on cleaned fused silica (Figure 3(a), i and ii). Then a 150 nm-wide gold grating with a height of 400 nm is patterned on the fused silica substrate

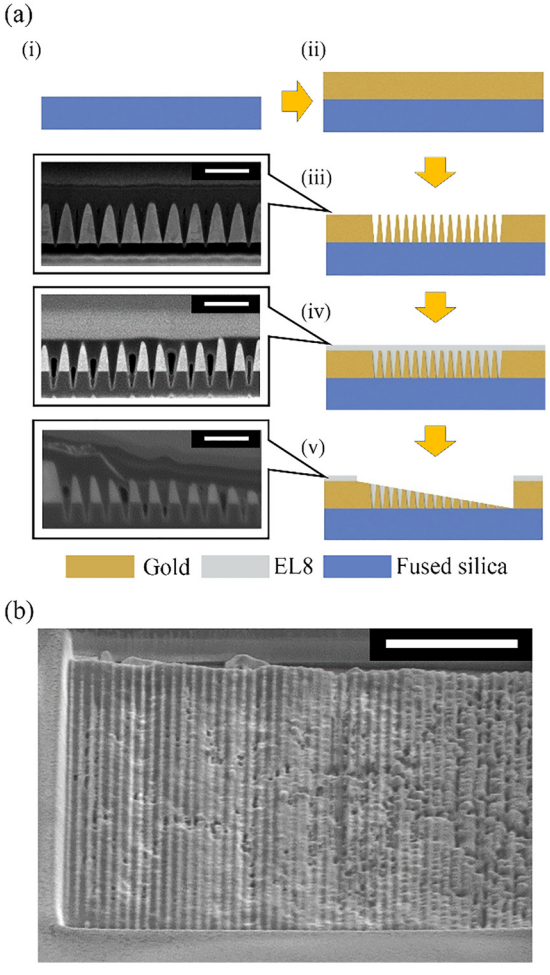


**Figure 3:** Fabrication of a vHMM.
(a) Fabrication process of a vHMM. (i) Preparation of a cleaned fused silica substrate; (ii) deposition of 400 nm-thick gold layer; (iii) first FIB milling to pattern the gold grating structures; (iv) spin-coating EL8; (v) second FIB milling to yield the final prism structure. Scale bar: 500 nm. (b) Scanning electron microscope image of the fabricated vHMM. Scale bar: 3 μm.

using FIB (Figure 3(a), iii) with a beam current of 80 pA for 10 min to cover the 10 $\mu m^2$ gold grating pattern. EL8 is spin-coated on the gold grating at 5000 rpm for 1 min and then baked at 90 °C for 5 min (Figure 3(a), iv). Finally, a gray-scale FIB milling process is conducted to fabricate prism vHMM structures (Figure 3(a), v). The fabricated vHMM (Figure 3(b)) has $d_m = 150$ and $d_d = 100$ nm, and $f = 0.4$. The height of the sample is 400 nm, so the AR is 4. The transmitted light propagates toward the refracted direction in the air, so the angle of refraction can be measured despite the short height of the vHMM (Figure 4(a)). Fabrication defects such as tilted sidewalls of fins and air gaps within the gold patterns can cause a discrepancy in measurement. The inclined sidewalls of fins are caused by the redeposition of sputtered materials during the FIB milling process [49, 50]. For low beam current during the process, the defect can be reduced [49, 50]. In addition, vacuum baking during the spin-coating process may reduce the air gap [51]. However, the tilted sidewall of the fin can create the hyperbolic shape of the isofrequency surface in a vHMM [15, 52], and the permittivity of the air gap is not much different from that of the resist to induce negative refraction.

## 4.2 Demonstration of negative refraction

The angle of refraction $\theta_r$ (Figure 4(a)) of the sample is measured at $\lambda$ = 450, 500, 550, 600, and 650 nm. $\theta_r$ is calculated using a charge-coupled device (CCD) camera to measure the position of the captured image pattern. The captured images are converted to intensity profiles (Figure 4(b)). If negative refraction occurs, the captured image pattern will appear to the left of the dashed line shown in Figure 4(b); as seen in images captured at $450 \le \lambda \le 550$ nm. The measured data demonstrates a similar trend to the simulated results (Figure 4(c)). The experimental results give $\theta_r = -0.40°$ at $\lambda = 450$ nm, $-1.03°$ at 500 nm, and $-0.69°$ at 550 nm. The angles of refraction are equivalent to those of negative-index metamaterials that have refractive indices of −0.18, −0.47, and −0.31 respectively. Because the $\tan\delta_\perp$ is sufficiently high, negative refraction is observed at $450 \le \lambda \le 550$ nm despite large $d_m/\lambda$ (Table 1). The simulated electric field profiles (Figure 4(d)) give $\theta_r = -1.4°$ at $\lambda = 450$ nm, $-1.61°$ at 500 nm, and $-0.41°$ at 550 nm when the structure is fabricated ideally. The negative phase propagation appears in the vHMM [5, 53]. Thus, light passing through the thicker part of the vHMM experiences phase advance compared with the other, and the transmitted light is refracted toward the negative direction. However, $\theta_r$ is 0.31° at $\lambda = 600$ nm, 0.50° at 650 nm. Because the absolute value of $\mathrm{Re}(\varepsilon_m)$ is

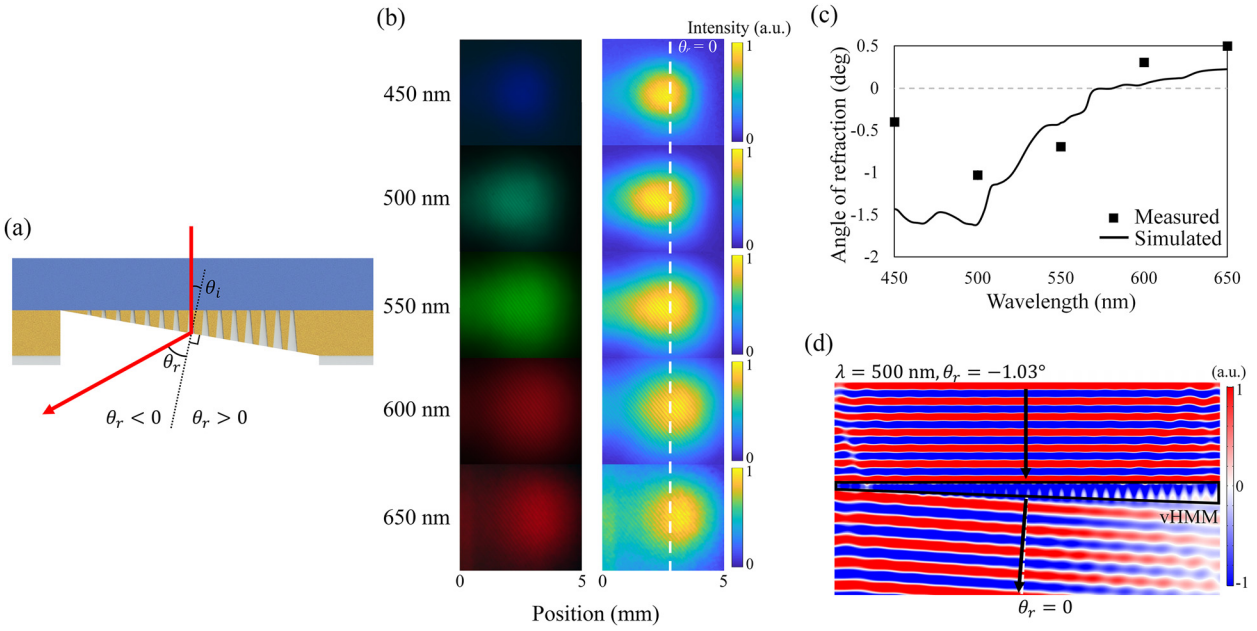


**Figure 4:** Observation of negative refraction.
(a) Schematic of negative refraction in a vHMM. If negative refraction occurs, the transmitted light propagates toward the left of the dashed line and the angle of refraction $\theta_r$ becomes negative. (b) Captured images (left) and the intensity profiles (right). The images are captured at the left side of the dashed line where negative refraction occurs. (c) Simulated and measured angles of refraction of the vHMM. Error bars are smaller than the point markers. (d) Simulated electric field profile at $\lambda$ = 500 nm. The simulated $\theta_r$ = –1.03°.

**Table 1:** Representative parameters of the vHMM.

| Wavelength (nm) | Angle of refraction (°) | Loss tangent (tan $\delta_\perp$ = Im($\varepsilon_\perp$)/Re($\varepsilon_\perp$)) | Ratio of structural geometry to wavelength ($d_m/\lambda$) |
|---|---|---|---|
| 450 | −0.40 ± 0.01 | 0.706 | 0.33 |
| 500 | −1.03 ± 0.01 | 1.08 | 0.30 |
| 550 | −0.69 ± 0.01 | 0.353 | 0.27 |
| 600 | 0.31 ± 0.01 | 0.0862 | 0.25 |
| 650 | 0.50 ± 0.01 | 0.0299 | 0.23 |

sufficiently larger than Im($\varepsilon_m$) at 600 ≤ $\lambda$ ≤ 650 nm, tan $\delta_\perp$ becomes too low and negative refraction is not observed, but Re($\varepsilon_\parallel$) and Im($\varepsilon_\parallel$) are independent to exhibit negative refraction [46]. At $\lambda$ = 650 nm, $d_m/\lambda$ is the smallest, but the tan $\delta_\perp$ is too low to observe negative refraction (Table 1).

## 4.3 Effect of diffraction

We consider the diffraction which may be in the vHMM (Figure 5). Because tangential components should be continuous at the interface, the transmitted angle $\theta_t$ of the diffracted light is expressed as

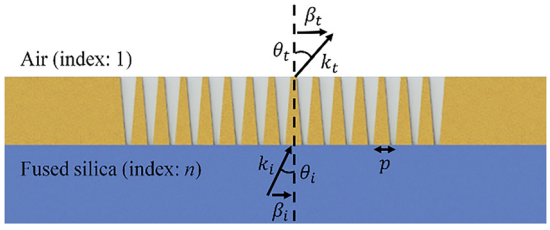


**Figure 5:** Schematic of diffraction in the vHMM. $\theta_t$ can be varied despite constant $\theta_i$ if the diffraction occurs. However, the diffraction is not valid in the vHMM because both $p$ and $\theta_i$ are sufficiently small.

$$\beta_t = \beta_i + \frac{2\pi m}{p}, \tag{6}$$

$$\beta_i = k_i \sin\theta_i = \frac{2\pi n}{\lambda}\sin\theta_i, \tag{7}$$

$$\beta_t = k_t \sin\theta_t = \frac{2\pi}{\lambda}\sin\theta_t, \tag{8}$$

$$\theta_t = \sin^{-1}\left(n\sin\theta_i + m\frac{\lambda}{p}\right), \tag{9}$$

where $m$ is an integer characterizing the diffractive modes, $k_i$ and $k_t$ are incident and transmitted wave vectors, respectively, $\beta_i$ and $\beta_t$ are transverse components of $k_i$ and $k_t$, respectively, $\theta_i$ is an incident angle, $n$ is a refractive index of the fused silica substrate, and $p$ is a period of the

vHMM. The argument of $\sin^{-1}$ in Equation (9) only has an absolute value smaller than unity at $m = 0$ because of both small $p$ ($\lambda/p \geq 1.8$) and $\theta_i$ ($\theta_i < 5°$) in our experiment. Therefore, we can conclude that the diffraction does not occur ($m = 0$) in the experiment.

# 5 Conclusions

In conclusion, we have experimentally demonstrated negative refraction using a vHMM composed of gold and EL8 without diffraction. The layers have thicknesses $d_m = 150$ nm and $d_d = 100$ nm, and the maximum height is 400 nm. AR is up to 4 and is realized using a commercial FIB milling process. The fabricated vHMM provides negative refraction at $\lambda = 450$, 500, and 550 nm, and which $\theta_r$ are −0.40°, −1.03°, and −0.69°, respectively. However, negative refraction is not observed at $\lambda = 600$ or 650 nm. The vHMM has sufficiently high enough $\tan \delta_\perp$ at $450 \leq \lambda \leq 550$ nm, so negative refraction occurs even though the ratio $d_m/\lambda$ is large. This result implies that the $\tan \delta_\perp$ of the vHMM is more dominant to exhibit hyperbolic dispersion and generate negative refraction than the ratio $d_m/\lambda$.

**Author contributions:** All the authors have accepted responsibility for the entire content of this submitted manuscript and approved submission.

**Research funding:** This work was financially supported by the POSCO-POSTECH-RIST Convergence Research Center program funded by POSCO, POSTECH-Samsung Semiconductor Research Center (IO201215-08187-01) funded by Samsung Electronics, and the National Research Foundation (NRF) grants (NRF-2019R1A2C3003129) funded by the Ministry of Science and ICT of the Korean government. Y.Y. acknowledges the Hyundai Motor Chung Mong-Koo fellowship, and the NRF fellowship (NRF-2021R1A6A3 A13038935) funded by the Ministry of Education (MOE) of the Korean government. S.S. acknowledges the NRF Global Ph.D. fellowship (NRF-2017H1A2A1043322) funded by the MOE of the Korean government.

**Conflict of interest statement:** The authors declare no conflicts of interest regarding this article.

# References

[1] A. Poddubny, I. Iorsh, P. Belov, and Y. Kivshar, "Hyperbolic metamaterials," *Nat. Photonics*, vol. 7, pp. 948–957, 2013.

[2] P. Shekhar, J. Atkinson, and Z. Jacob, "Hyperbolic metamaterials: fundamentals and applications," *Nano Converg.*, vol. 1, p. 14, 2014.

[3] Z. Guo, H. Jiang, and H. Chen, "Hyperbolic metamaterials: from dispersion manipulation to applications," *J. Appl. Phys.*, vol. 127, p. 071101, 2020.

[4] O. Takayama and A. V. Lavrinenko, "Optics with hyperbolic materials," *J. Opt. Soc. Am. B*, vol. 36, p. F38, 2019.

[5] J. Valentine, S. Zhang, T. Zentgraf, et al., "Three-dimensional optical metamaterial with a negative refractive index," *Nature*, vol. 455, pp. 376–379, 2008.

[6] A. A. Orlov, S. V. Zhukovsky, I. V. Iorsh, and P. A. Belov, "Controlling light with plasmonic multilayers," *Photonics Nanostruct. Fundam. Appl.*, vol. 12, pp. 213–230, 2014.

[7] S. Xiao, U. K. Chettiar, A. V. Kildishev, V. P. Drachev, and V. M. Shalaev, "Yellow-light negative-index metamaterials," *Opt. Lett.*, vol. 34, pp. 3478–3480, 2009.

[8] C. García-Meca, J. Hurtado, J. Martí, A. Martínez, W. Dickson, and A. V. Zayats, "Low-loss multilayered metamaterial exhibiting a negative index of refraction at visible wavelengths," *Phys. Rev. Lett.*, vol. 106, p. 067402, 2011.

[9] J. Zhang, H. Jiang, B. Gralak, S. Enoch, G. Tayeb, and M. Lequime, "Towards -1 effective index with one-dimensional metal-dielectric metamaterial: A quantitative analysis of the role of absorption losses," *Opt. Express*, vol. 15, pp. 7720–7729, 2007.

[10] G. V. Naik, J. Liu, A. V. Kildishev, V. M. Shalaev, and A. Boltasseva, "Demonstration of Al:ZnO as a plasmonic component for near-infrared metamaterials," *Proc. Natl. Acad. Sci. U. S. A*, vol. 109, pp. 8834–8838, 2012.

[11] A. J. Hoffman, L. Alekseyev, S. S. Howard, et al., "Negative refraction in semiconductor metamaterials," *Nat. Mater.*, vol. 6, pp. 946–950, 2007.

[12] K. G. Eyink, H. J. Haugan, A. T. Neal, K. Mahalingam, V. Pustovit, and A. Urbas, "Determination of critical parameters for design of semiconductor hyperbolic metamaterials," *Opt. Mater.*, vol. 112, p. 110576, 2021.

[13] A. Hierro, M. Montes Bajo, M. Ferraro, et al., "Optical phase transition in semiconductor quantum metamaterials," *Phys. Rev. Lett.*, vol. 123, p. 117401, 2019.

[14] H. N. S. Krishnamoorthy, B. Gholipour, N. I. Zheludev, and C. Soci, "A non-volatile chalcogenide switchable hyperbolic metamaterial," *Adv. Opt. Mater.*, vol. 6, p. 1800332, 2018.

[15] A. A. High, R. C. Devlin, A. Dibos, et al., "Visible-frequency hyperbolic metasurface," *Nature*, vol. 522, pp. 192–196, 2015.

[16] M. Kim, S. So, K. Yao, Y. Liu, and J. Rho, "Deep sub-wavelength nanofocusing of UV-visible light by hyperbolic metamaterials," *Sci. Rep.*, vol. 6, p. 38645, 2016.

[17] M. Byun, D. Lee, M. Kim, et al., "Demonstration of nanoimprinted hyperlens array for high-throughput sub-diffraction imaging," *Sci. Rep.*, vol. 7, p. 46314, 2017.

[18] D. Lee, M. Kim, S. So, et al., "Demonstration of a hyperlens-integrated microscope and super-resolution imaging," *J. Vis. Exp.*, vol. 127, p. e55968, 2017.

[19] D. Lee, J. Gwak, T. Badloe, S. Palomba, and J. Rho, "Metasurfaces-based imaging and applications: from miniaturized optical components to functional imaging platforms," *Nanoscale Adv.*, vol. 2, pp. 605–625, 2020.

[20] S. So and J. Rho, "Geometrically flat hyperlens designed by transformation optics," *J. Phys. D Appl. Phys.*, vol. 51, p. 194003, 2019.

[21] C. W. Tao, T. J. Yen, and T. Y. Huang, "Achieving sub-wavelength imaging through a flat hyperlens in a modified anodic aluminum oxide template," *Sci. Rep.*, vol. 10, p. 5296, 2020.

[22] Y. U. Lee, J. Zhao, G. C. H. Mo, et al., "Metamaterial-assisted photobleaching microscopy with nanometer scale axial resolution," *Nano Lett*, vol. 20, pp. 6038–6044, 2020.
[23] Y. U. Lee, C. Posner, J. Zhao, J. Zhang, and Z. Liu, "Imaging of cell morphology changes via metamaterial-assisted photobleaching microscopy," *Nano Lett.*, vol. 21, pp. 1716–1721, 2021.
[24] Y. U. Lee, J. Zhao, Q. Ma, et al., "Metamaterial assisted illumination nanoscopy via random super-resolution speckles," *Nat. Commun.*, vol. 12, p. 1559, 2021.
[25] M. Kim, D. Lee, T. H. Kim, Y. Yang, H. J. Park, and J. Rho, "Observation of enhanced optical spin Hall effect in a vertical hyperbolic metamaterial," *ACS Photonics*, vol. 6, pp. 2530–2536, 2019.
[26] O. Takayama, J. Sukham, R. Malureanu, A. V. Lavrinenko, and G. Puentes, "Photonic spin Hall effect in hyperbolic metamaterials at visible wavelengths," *Opt. Lett.*, vol. 43, p. 4602, 2018.
[27] X. Yang, J. Yao, J. Rho, X. Yin, and X. Zhang, "Experimental realization of three-dimensional indefinite cavities at the nanoscale with anomalous scaling laws," *Nat. Photonics*, vol. 6, pp. 450–454, 2012.
[28] Y. Guo, C. L. Cortes, S. Molesky, and Z. Jacob, "Broadband super-planckian thermal emission from hyperbolic metamaterials," *Appl. Phys. Lett.*, vol. 101, p. 131106, 2013.
[29] P. N. Dyachenko, S. Molesky, A. Y. Petrov, et al., "Controlling thermal emission with refractory epsilon-near-zero metamaterials via topological transitions," *Nat. Commun.*, vol. 7, p. 11809, 2016.
[30] S. Hu, S. Du, J. Li, and C. Gu, "Multidimensional image and beam splitter based on hyperbolic metamaterials," *Nano Lett.*, vol. 21, pp. 1792–1799, 2021.
[31] A. Calzolari, A. Catellani, M. Buongiorno Nardelli, and M. Fornari, "Hyperbolic metamaterials with extreme mechanical hardness," *Adv. Opt. Mater.*, vol. 9, p. 2001904, 2021.
[32] E. Shkondin, T. Repän, M. E. Aryaee Panah, A. V. Lavrinenko, and O. Takayama, "High aspect ratio plasmonic nanotrench structures with large active surface area for label-free mid-infrared molecular absorption sensing," *ACS Appl. Nano Mater.*, vol. 1, pp. 1212–1218, 2018.
[33] J. Wu, F. Wu, C. Xue, et al., "Wide-angle ultrasensitive biosensors based on edge states in heterostructures containing hyperbolic metamaterials," *Opt. Express*, vol. 27, pp. 24835–24846, 2019.
[34] K. V. Sreekanth, Y. Alapan, M. Elkabbash, et al., "Extreme sensitivity biosensing platform based on hyperbolic metamaterials," *Nat. Mater.*, vol. 15, pp. 621–627, 2016.
[35] K. V. Sreekanth, Y. Alapan, M. ElKabbash, et al., "Enhancing the angular sensitivity of plasmonic sensors using hyperbolic metamaterials," *Adv. Opt. Mater.*, vol. 4, pp. 1767–1772, 2016.
[36] T. A. Chen, I. W. Un, C. C. Wei, Y. J. Lu, D. P. Tsai, and T. J. Yen, "Alternating nanolayers of dielectric MgF2and metallic Ag as hyperbolic metamaterials: probing surface states and optical topological phase transition and implications for sensing applications," *ACS Appl. Nano Mater.*, vol. 4, pp. 2211–2217, 2021.
[37] O. Takayama, E. Shkondin, A. Bodganov, et al., "Midinfrared surface waves on a high aspect ratio nanotrench platform," *ACS Photonics*, vol. 4, pp. 2899–2907, 2017.
[38] M. Mahmoodi, S. H. Tavassoli, O. Takayama, J. Sukham, R. Malureanu, and A. V. Lavrinenko, "Existence conditions of high-k modes in finite hyperbolic metamaterials," *Laser Photonics Rev.*, vol. 13, pp. 1–12, 2019.
[39] Y. Feng, Z. Da. Hu, A. Balmakou, et al., "Perfect narrowband absorber based on patterned graphene-silica multilayer hyperbolic metamaterials," *Plasmonics*, vol. 15, pp. 1869–1874, 2020.
[40] J. K. Behera, K. Liu, M. Lian, and T. Cao, "A reconfigurable hyperbolic metamaterial perfect absorber," *Nanoscale Adv.*, vol. 3, pp. 1758–1766, 2021.
[41] J. Elser, R. Wangberg, V. A. Podolskiy, and E. E. Narimanov, "Nanowire metamaterials with extreme optical anisotropy," *Appl. Phys. Lett.*, vol. 89, p. 261102, 2006.
[42] S. Tang, B. Zhu, M. Jia, et al., "Effective-medium theory for one-dimensional gratings," *Phys. Rev. B Condens. Matter*, vol. 91, p. 174201, 2015.
[43] S. Bang, S. So, and J. Rho, "Realization of broadband negative refraction in visible range using vertically stacked hyperbolic metamaterials," *Sci. Rep.*, vol. 9, p. 14093, 2019.
[44] E. Shkondin, T. Repän, O. Takayama, and A. V. Lavrinenko, "High aspect ratio titanium nitride trench structures as plasmonic biosensor," *Opt. Mater. Express*, vol. 7, pp. 4171–4182, 2017.
[45] I. Murataj, M. Channab, E. Cara, et al., "Hyperbolic metamaterials via hierarchical block copolymer nanostructures," *Adv. Opt. Mater.*, vol. 9, p. 2001933, 2021.
[46] H. Cho, S. So, T. Badloe, S. Bang, and J. Rho, "Critical layer thickness analysis of vertically stacked hyperbolic metamaterials for effective negative refraction generation," *Adv. Theory Simul.*, vol. 3, p. 2000138, 2020.
[47] V. M. Agranovich and V. E. Kravtsov, "Notes on crystal optics of superlattices," *Solid State Commun.*, vol. 55, pp. 85–90, 1985.
[48] C. Zhang, N. Hong, C. Ji, et al., "Robust extraction of hyperbolic metamaterial permittivity using total internal reflection ellipsometry," *ACS Photonics*, vol. 5, pp. 2234–2242, 2018.
[49] W. C. L. Hopman, F. Ay, W. Hu, et al., "Focused ion beam scan routine, dwell time and dose optimizations for submicrometre period planar photonic crystal components and stamps in silicon," *Nanotechnology*, vol. 18, p. 195305, 2007.
[50] S. Lipp, L. Frey, C. Lehrer, B. Frank, E. Demm, and H. Ryssel, "Investigations on the topology of structures milled and etched by focused ion beams," *J. Vac. Sci. Technol. B*, vol. 14, pp. 3996–3999, 1996.
[51] T. Yoshikawa, T. Konishi, M. Nakajima, H. Kikuta, H. Kawata, and Y. Hirai, "Fabrication of 1/4 wave plate by nanocasting lithography," *J. Vac. Sci. Technol. B*, vol. 23, pp. 2939–2943, 2005.
[52] Z. Li, J. S. T. Smalley, R. Haroldson, et al., "Active perovskite hyperbolic metasurface," *ACS Photonics*, vol. 7, pp. 1754–1761, 2020.
[53] J. B. Pendry, "Negative refraction makes a perfect lens," *Phys. Rev. Lett.*, vol. 85, pp. 3966–3969, 2000.